Quantum Information Processing manuscript No.
(will be inserted by the editor)

The excitonic qubit on a star graph: dephasing-limited coherent motion

Vincent Pouthier

Received: date / Accepted: date

Abstract A phenomenological model is used for describing how a fluctuating bath modifies the way an exciton promotes quantum state transfer on a star graph. A markovian generalized master equation is first established. Then, it is solved exactly for studying specific elements of the exciton reduced density matrix. These elements, called coherences, characterize the ability of the exciton to develop qubit states that are superimpositions involving the vacuum and the local one-exciton states. Although dephasing-limited coherent motion is clearly evidenced, it is shown that both the decoherence and the information transfer are very sensitive to the number of branches that form the star. The larger the branch number is, the slower is the decoherence and the better is the efficiency of the transfer.

Keywords Exciton · Star Graph · Decoherence · Quantum State Transfer

1 Introduction

At nanoscale, solid-state based communication protocols are one of the best candidates to promote the transfer of qubit states, a fundamental task in quantum information processing. This quantum state transfer (QST) is needed to ensure a perfect communication between the different parts of a computer or between neighboring computers [1]. The interest of using nano-structures in scalable computing is twofold [2]. First, the qubits are encoded on elementary excitations that naturally propagate along the lattice due to the inherent interactions between sites. QST is thus spontaneously achieved without any external control. Second, no interfacing is required between the computer and the data bus, both involving the same elementary excitations. Owing to the wide variety of collective excitations that arise in condensed matter, different protocols have been proposed during the last decade. Examples among many involve spin networks [3–5], quantum dots

V. Pouthier
Institut UTINAM, Université de Franche-Comté, CNRS UMR 6213, 25030 Besançon, France.
E-mail: vincent.pouthier@univ-fcomte.fr

[6], optical lattices [7], trapped ions [8], conducting polymers [9], phonons in low-dimensional crystals [10] and vibrons in molecular nanowires [11–13].

Recently, it has been suggested that exciton-mediated QST in dendrimers could be a promising way for quantum information processing [14–18]. A dendrimer is an engineered hyperbranched polymer whose self-similar geometry at nanoscale resembles to the fractal patterns that occur in the plant kingdom [19]. It exhibits a central core to which several dendritic branches are attached. Therefore, in a typical communication protocol, the periphery of the molecule plays the role of a computer where the information is implemented whereas the central core is occupied by a second computer where the information is received. Of course, one can consider the reverse situation. The communication between the two computers is thus mediated by an excitonic wave that propagates along the dendritic branches. Note that at the origin, it has been pointed out that dendrimers could behave as artificial light-harvesting complexes able to convert the energy of a radiation into a chemical fuel [20].

In fact, exciton-mediated QST in dendrimers is a special case of a more general subject devoted to the characterization of the excitonic propagation in complex networks. This characterization is of fundamental importance because of the formal resemblance between the exciton dynamics and a continuous time quantum walk (CTQW) [16]. During the past few years, CTQW in complex networks has become a very popular research topic owing to its potential use in the development of quantum algorithms [21–24]. Consequently, it has been studied in a great variety of networks including binary and glued trees [24–26], Apollonian networks [27,28], and star graphs [29–32], to cite but a few examples.

In that context, the previous examples clearly show that the coherent propagation of an excitonic qubit in a complex network could play a key role in quantum information processing. Unfortunately, in a realistic nano-structures, the exciton does not propagate freely. It interacts with the remaining degrees of freedom of the medium that usually form a thermal bath responsible for dephasing or quantum decoherence [33,34]. In a regular lattice, dephasing-limited coherent motion prevents the occurrence of any high-fidelity QST nor efficient CTQW [35]. Therefore, the fundamental question arises whether the specific topology of a complex network modifies the dephasing processes.

To answer that question, this work presents a phenomenological model for studying the dephasing mechanisms that affect the exciton dynamics in a star graph. To proceed, dissipative effects will be treated using a stochastic approach in which the thermal bath induces random fluctuations of the dynamical parameters that control the excitonic propagation (see for instance Refs. [36–40]). Note that the choice of the star graph is not the result of chance. Indeed, this graph is one of the most regular structures in graph theory. Organized around a central core, it exhibits the local tree structure of irregular and complex networks and it formally looks like a dendrimer. However, its topology remains sufficiently simple so that analytical calculations can be carried out exactly. The present work can thus be viewed as a first step and more realistic situations will be addressed in forthcoming papers.

The paper is organized as follows. In Sect. 2, the star graph is described and the exciton-bath Hamiltonian is defined. Then, QST is formulated in terms of the excitonic coherences that refer to specific elements of the exciton reduced density matrix. A generalized master equation is established for describing the dynamics

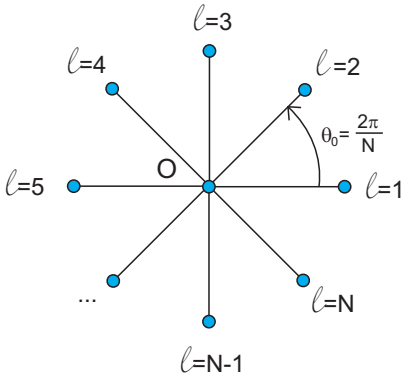

Fig. 1 Representation of the star graph S_N with $N+1$ nodes $\ell = 0, ..., N$ and N branches.

of the coherences. Finally, the master equation is solved analytically in Sect. 3 where the corresponding solutions are presented and discussed.

2 Theoretical background

2.1 Model Hamiltonian

The system we consider is the star graph S_N illustrated in Fig. 1. It corresponds to a tree with $N+1$ nodes formed by N branches that emanate out from a central core. The central core, labeled by the index $\ell = 0$, is thus connected to N branch sites $\ell = 1, ..., N$. Each site $\ell = 0, ..., N$ is occupied by a molecular subunit whose internal (i.e. electronic or vibrational) dynamics is described by a two-level system. Let ω_0 stand for the corresponding Bohr frequency and let $|\ell\rangle$ denote the state in which the ℓth two-level system occupies its first excited state, the other two-level systems remaining in their ground state. The vacuum state $|\oslash\rangle$ describes all the two-level systems in their ground state. The exciton Hamiltonian that governs both the zero- and the one-exciton dynamics is thus defined in terms of the exciton hopping constant Φ as (the convention $\hbar = 1$ will be used throughout this paper)

$$H_A = \sum_{\ell=0}^{N} \omega_0 |\ell\rangle\langle\ell| + \sum_{\ell=1}^{N} \Phi(|0\rangle\langle\ell| + |\ell\rangle\langle 0|) \tag{1}$$

Different strategies have been developed for describing the one-exciton eigenstates [29–31]. Here, we take advantage of the fact that H_A possesses discrete rotational symmetry. It remains invariant under the discrete rotation of angle $\theta_0 = 2\pi/N$ and centered on the core site $\ell = 0$. Consequently, its diagonalization is greatly simplified when one works with the so-called Bloch basis [41] that involves the local state $|\ell = 0\rangle$ and N orthogonal Bloch states $|\chi_k\rangle$ $(k = 1, ..., N)$ defined as

$$|\chi_k\rangle = \frac{1}{\sqrt{N}} \sum_{\ell=1}^{N} e^{ik\ell\theta_0} |\ell\rangle \tag{2}$$

Within the Bloch basis, the star graph exhibits two kinds of eigenstates. First, the spectrum of the graph shows the $(N-1)$-fold degenerate eigenenergy ω_0, the corresponding eigenstates being the $N-1$ Bloch states $|\chi_k\rangle$, with $k=1,...,N-1$. Second, the graph supports two eigenstates $|\chi_\pm\rangle$ that correspond to superimpositions involving the state $|0\rangle$ and the Bloch state $|\chi_N\rangle$ that is uniformly distributed over the periphery of the star. These eigenstates are defined as

$$|\chi_\pm\rangle = \frac{1}{\sqrt{2}}(|0\rangle \pm |\chi_N\rangle) \tag{3}$$

the corresponding eigenenergy being $\omega_\pm = \omega_0 \pm \sqrt{N}\Phi$. These $N+1$ eigenstates describe an exciton that propagates along the star graph. This propagation is accounted by the free propagator $G(t) = \exp(-iH_A t)$ that is formally expressed as

$$\begin{aligned} G(t) = \mathbf{1}e^{-i\omega_0 t} &- (|0\rangle\langle 0| + |\chi_N\rangle\langle\chi_N|)\left(1-\cos(\sqrt{N}\Phi t)\right)e^{-i\omega_0 t} \\ &- i(|0\rangle\langle\chi_N| + |\chi_N\rangle\langle 0|)\sin(\sqrt{N}\Phi t)e^{-i\omega_0 t} \end{aligned} \tag{4}$$

where $\mathbf{1}$ is the identity operator.

At this step, let us mention that a detailed study of the exciton propagator allows us to bring out the general features that characterize the complex network dynamics [16]. The two main results are as follows. When the exciton wave function is initially uniformly distributed over the periphery or localized on the central core, it delocalizes coherently between the periphery and the core. The exciton dynamics is thus mapped onto that of a two-site system whose the effective hopping constant is $\sqrt{N}\Phi$. By contrast, when the exciton is initially located on a single branch site, it tends to remain confined over the excited site. A localization takes place due to the specific quantum self-interferences that arise because the star graph supports a $(N-1)$-fold degenerate eigenenergy.

Unfortunately, the exciton does not evolve freely but it interacts with the remaining degrees of freedom of the star. They form a thermal bath whose dynamics is governed by the Hamiltonian H_B. This interaction results from a stochastic modulation of the Bohr frequency of each two-level system induced by the motions of the bath. The corresponding coupling Hamiltonian is defined as

$$\Delta H = \sum_{\ell=0}^{N} \Delta\omega_\ell |\ell\rangle\langle\ell| \tag{5}$$

where $\Delta\omega_\ell$ is an operator that depends only on the bath degrees of freedom.

The exciton-bath dynamics is thus governed by the full Hamiltonian $H = H_A + H_B + \Delta H$ which will be used to study the properties of an excitonic qubit. Since H is an exciton number conserving Hamiltonian, the Hilbert space is partitioned into independent subspaces $\mathcal{E} = \mathcal{E}_0 \oplus \mathcal{E}_1$, where $\mathcal{E}_v$ denotes the v-exciton subspace. The coupling ΔH vanishes in $\mathcal{E}_0$ whereas it turns on in $\mathcal{E}_1$. Therefore, a qubit state corresponding to a superimposition of states belonging to the zero- and to the one-exciton subspace, the coupling ΔH will produce quantum decoherence that strongly affects QST, as shown in the following of the paper.

2.2 Excitonic coherences and QST

Without any perturbation, the star graph is supposed to be in thermal equilibrium at temperature T. Assuming that $\omega_0 \gg k_B T$ (k_B is the Boltzmann constant), all the two-level systems are in their ground state. This is no longer the case for the thermal bath whose eigenstates are not well defined. Its properties are thus encoded in the standard Boltzmann density matrix $\rho_B = \exp(-\beta H_B)/Z_B$, Z_B being the bath partition function ($\beta = 1/k_B T$). In that context, for describing the exciton dynamics, the star must be brought into a configuration out of equilibrium in which the exciton is prepared in a state $|\psi_A\rangle \neq |\oslash\rangle$. This step is supposed to be rather fast when compared with the typical time evolution of the thermal bath. Therefore, after this initial preparation, the full system becomes described by the density matrix $\rho(0) = |\psi_A\rangle\langle\psi_A| \otimes \rho_B$.

To study exciton-mediated QST, one chooses $|\psi_A\rangle$ as a qubit implemented on the molecular group ℓ_0 as

$$|\psi_A\rangle = \alpha|\oslash\rangle + \beta|\ell_0\rangle \tag{6}$$

where $|\alpha|^2 + |\beta|^2 = 1$. Our aim is thus to measure the ability of the system to freely evolve in time so that this initial qubit is copied on a second site ℓ. Whatever its duration, QST must be realized with the largest fidelity despite the coupling with the thermal bath. To define this fidelity measure, different objects have been introduced [42], one of the most widely used being certainly the so-called average Schumacher's fidelity [3]. Here, we restrict our attention to the excitonic coherences. Indeed, the exciton properties are encoded in the reduced density matrix (RDM) $\sigma(t) = Tr_B[\rho(t)]$, where Tr_B is a partial trace over the bath degrees of freedom. The coherences are thus the off-diagonal matrix elements $\sigma_\ell(t) = \langle\ell|\sigma(t)|\oslash\rangle$. They provide information about the ability of the ℓth two-level system to develop a superimposition between its ground state and its first excited state a time t. They are defined as

$$\sigma_\ell(t) = \langle\ell|Tr_B\left[\rho_B e^{iH_B t} e^{-iHt}\right]|\ell_0\rangle\sigma_{\ell_0}(0) \tag{7}$$

where $\sigma_{\ell_0}(0) = \alpha^*\beta$.

The excitonic coherence generalizes the concept of transition amplitude. It yields the probability amplitude to observe the exciton in $|\ell\rangle$ at time t given that it was in $|\ell_0\rangle$ at $t = 0$. Its effective nature results from the fact that the exciton interacts with the bath during its transition. The excitonic coherence is the central object of the present study. The condition $|\sigma_\ell(t)/\sigma_{\ell_0}(0)| = 1$ reveals that the ℓth site reaches a state at time t that is equivalent to the initial state, to a phase factor. Note that this condition is exactly the QST fidelity when the coupling with the bath is disregarded [3]. Consequently, depending on the value of the model parameters, studying the maximum value of $|\sigma_\ell(t)|$ provides key information about the fidelity of the QST.

2.3 Generalized Master Equation

For characterizing the time evolution of the excitonic coherences, we use a standard projector technique (see for instance Refs. [33,34]). This method has demonstrated

its usefulness in eliminating irrelevant information from a system (the bath dynamics), and extracting only the information that is desired (the coherence dynamics). To proceed, a second-order perturbation theory with respect to the coupling ΔH is performed (Born approximation) and the Markov approximation is applied. The generalized master equation (GME) for the coherences is thus written as [35]

$$i\dot{\sigma}_\ell(t) = \sum_{\ell'=0}^{N} (H_{A\ell\ell'} - i\mathcal{R}_{\ell\ell'})\sigma_{\ell'}(t) \tag{8}$$

The first term in the right-end-side of equation (8) describes the free evolution of the coherences under the influence of the exciton Hamiltonian H_A, only. By contrast, the effect of the thermal bath is encoded in the relaxation operator whose matrix elements are written in terms of the free exciton propagator as

$$\mathcal{R}_{\ell,\ell'} = \sum_{\ell''} \int_0^\infty d\tau \; C_{\ell,\ell''}(\tau) G_{\ell,\ell'}(\tau) G^*_{\ell',\ell''}(\tau) \tag{9}$$

As shown in equation (9), the influence of the bath is captured in the exciton-bath coupling correlation function $C_{\ell,\ell'}(t) = \langle \Delta\omega_\ell(t)\Delta\omega_{\ell'}(0)\rangle_B$. The symbol $\langle ...\rangle_B$ is an average over the bath degrees of freedom and the time dependence of $\Delta\omega_\ell$ results from an Heisenberg representation with respect to H_B. Note that the mean value $\langle \Delta\omega_\ell(t)\rangle_B$ is assumed to be zero.

Basically two approaches have been developed in the literature for determining the correlation functions. Within the first approach, known as the potential deformation model, the thermal bath is described in terms of the collective vibrations (phonons) of the host medium. The coupling ΔH is thus expressed as a linear expansion of the corresponding vibrational coordinates so that $C_{\ell,\ell'}(t)$ can be evaluated exactly [33].

Here, we shall follow the second approach in which the couplings $\Delta\omega_\ell(t)$ are viewed as stochastic variables [36–40]. Within this approach, a detailed description of the fluctuating bath is not required. The influence of the bath is encoded in the second order correlation functions that are chosen phenomenologically to recover the typical behavior of the real correlations. In that context, it is usually assumed that the correlations decay faster than any other time scale of the system. Therefore, the variables $\Delta\omega_\ell(t)$ behave as a Gaussian white noise with zero mean and delta correlations. However, as pointed recently, such an assumption is often "too strong" for excitonic problem and it is necessary to account for the fact that the correlations decay over a finite time scale. To overcome this problem, we thus follow Silbey and co-workers [40] and assume that the couplings $\Delta\omega_\ell(t)$ are independent variables with zero mean and whose correlation function $C(t) = \langle \Delta\omega_\ell(t)\Delta\omega_{\ell'}(0)\rangle_B \delta_{\ell\ell'}$ shows an exponential decay for all ℓ expressed as

$$C(t) = \frac{\gamma}{\tau_c} \exp(-t/\tau_c) \tag{10}$$

In equation (10), τ_c stands for the correlation time of the thermal bath and γ provides a measure of the strength of the coupling between the exciton and the bath.

From the knowledge of both the exciton propagator (equation (4)) and the coupling correlation function (equation (10)), we are able to compute the relaxation

operator. In doing so, it is straightforward to show that the relaxation operator exhibits only five kinds of matrix elements. Three kinds of elements define real components that account for quantum decoherence. The first element $\Gamma_C = \mathcal{R}_{00}$ is the dephasing rate of the core state $|0\rangle$. For all $\ell \neq 0$, the second kind of elements $\Gamma_B = \mathcal{R}_{\ell\ell}$ is the dephasing rate of each branch state $|\ell\rangle$ that belongs to the periphery of the star. For all $\ell \neq \ell' \neq 0$, the last kind of real elements is defined as $\Gamma_I = \mathcal{R}_{\ell\ell'}$. Two kinds of elements define imaginary components that account for the correction of the exciton hopping constant. For all $\ell \neq 0$, the corresponding elements are $\Delta_C = -i\mathcal{R}_{0\ell}$ and $\Delta_B = -i\mathcal{R}_{\ell 0}$. Note that these corrections break the symmetric nature of the exciton hops between the core and the periphery of the star. After straightforward calculations, one finally obtains

$$\begin{aligned}
\Gamma_C &= \gamma \left(\frac{1+2NB^2}{1+4NB^2} \right) \\
\Gamma_B &= \frac{\gamma}{N^2} \left((N-1)^2 + \frac{2(N-1)}{1+NB^2} + \frac{1+2NB^2}{1+4NB^2} \right) \\
\Gamma_I &= \frac{\gamma}{N^2} \left(-(N-1) + \frac{N-2}{1+NB^2} + \frac{1+2NB^2}{1+4NB^2} \right) \\
\Delta_C &= \left(\frac{\gamma B}{1+4NB^2} \right) \\
\Delta_B &= \left(\frac{N-1}{N} \frac{\gamma B}{1+NB^2} + \frac{1}{N} \frac{\gamma B}{1+4NB^2} \right)
\end{aligned} \tag{11}$$

where $B = \Phi\tau_c$ defines the so-called adiabaticity, that is the ratio between the thermal bath correlation time τ_c and the typical time evolution of the excitonic wave Φ^{-1}.

From the knowledge of the relaxation operator, the GME in the local basis is thus expressed as

$$\begin{aligned}
i\dot{\sigma}_\ell(t) &= (\omega_0 - i\Gamma_B)\sigma_\ell(t) + (\Phi + \Delta_B)\sigma_0(t) - i\Gamma_I \sum_{\ell'=1}^{N} \sigma_{\ell'}(t)(1-\delta_{\ell'\ell}) \quad \forall \ell \neq 0 \\
i\dot{\sigma}_0(t) &= (\omega_0 - i\Gamma_C)\sigma_0(t) + (\Phi + \Delta_C) \sum_{\ell=1}^{N} \sigma_\ell(t)
\end{aligned} \tag{12}$$

Equation (12) reveals that the GME is isomorphic to the Schrodinger equation for a single exciton moving on the star graph. The coherence plays the role of a wave function whose dynamics is governed by the effective non-hermitian Hamiltonian $\mathcal{H} = H_A - i\mathcal{R}$ that breaks the unitary nature of the quantum dynamics. The imaginary part of the relaxation operator defines the non symmetric corrections to the exciton Hamiltonian whereas its real part accounts for dephasing processes. However, the key point is that the effective Hamiltonian conserves the rotational symmetry of the star graph so that it remains invariant under the discrete rotation of angle $\theta_0 = 2\pi/N$ and centered on the core site $\ell = 0$. Therefore, the GME can be solved exactly by performing a Bloch transformation based on the introduction of N new variables defined as

$$\tilde{\sigma}_k(t) = \frac{1}{\sqrt{N}} \sum_{\ell=1}^{N} e^{-ik\ell\theta_0} \sigma_\ell(t) \quad \forall k = 1, ..., N \tag{13}$$

By applying the Bloch transformation, the GME becomes

$$\begin{aligned} i\dot{\tilde{\sigma}}_k(t) &= (\omega_0 - i\gamma_0)\tilde{\sigma}_k(t) \quad \forall k = 1, ..., N-1 \\ i\dot{\tilde{\sigma}}_N(t) &= (\omega_0 - i\gamma_B)\tilde{\sigma}_N(t) + \Phi_B\sigma_0(t) \\ i\dot{\sigma}_0(t) &= (\omega_0 - i\Gamma_C)\sigma_0(t) + \Phi_C\tilde{\sigma}_N(t) \end{aligned} \tag{14}$$

where $\gamma_B = \Gamma_B + (N-1)\Gamma_I$, $\gamma_0 = \Gamma_B - \Gamma_I$, $\Phi_C = \sqrt{N}(\Phi + \Delta_C)$ and $\Phi_B = \sqrt{N}(\Phi + \Delta_B)$. The Bloch transformation allows us to partially decouple the evolution of the excitonic coherences. Within this new point of view, the GME first involves $(N-1)$ independent and isomorphic equations that describe the time evolution of the coherence $\tilde{\sigma}_k(t)$ of the Bloch states $k = 1, ..., N-1$. Then, the two remaining equations define a system of coupled equations. It characterizes the interaction between the coherent $\sigma_0(t)$ of the core site and the coherence $\tilde{\sigma}_N(t)$ of the Bloch state uniformly distributed over the periphery of the star. The solution of this GME is thus obtained from the diagonalization of the corresponding effective Hamiltonian. This diagonalization reveals that the exciton dynamics is characterized by three different effective eigenenergies z_0 and $z_\pm$ defined as

$$\begin{aligned} z_0 &= \omega_0 - i\gamma_0 \\ z_\pm &= \omega_0 \pm \Omega - i\bar{\Gamma} \end{aligned} \tag{15}$$

where $\bar{\Gamma} = (\gamma_B + \Gamma_C)/2$, $\bar{\gamma} = (\gamma_B - \Gamma_C)/2$, and $\Omega = \sqrt{\Phi_B\Phi_C - \bar{\gamma}^2}$. The $(N-1)$-fold degenerate effective energy z_0 describes the damped oscillations of the coherences $\tilde{\sigma}_k(t)$ with $k = 1, ..., N-1$ whereas $z_\pm$ account for the coherence exchanges between the core and the periphery of the star.

From the knowledge of the initial conditions, the GME equation (14) can be solved exactly. One thus obtains

$$\begin{aligned} \tilde{\sigma}_k(t) &= \tilde{\sigma}_k(0)e^{-i\omega_0 t}e^{-\gamma_0 t} \quad \forall k = 1, ..., N-1 \\ \tilde{\sigma}_N(t) &= \frac{1}{2}\left[\left(1 - i\frac{\bar{\gamma}}{\Omega}\right)\tilde{\sigma}_N(0) + \frac{\Phi_B}{\Omega}\sigma_0(0)\right]e^{-iz_+ t} \\ &\quad + \frac{1}{2}\left[\left(1 + i\frac{\bar{\gamma}}{\Omega}\right)\tilde{\sigma}_N(0) - \frac{\Phi_B}{\Omega}\sigma_0(0)\right]e^{-iz_- t} \\ \sigma_0(t) &= \frac{1}{2}\left[\left(1 + i\frac{\bar{\gamma}}{\Omega}\right)\sigma_0(0) + \frac{\Phi_C}{\Omega}\tilde{\sigma}_N(0)\right]e^{-iz_+ t} \\ &\quad + \frac{1}{2}\left[\left(1 - i\frac{\bar{\gamma}}{\Omega}\right)\sigma_0(0) - \frac{\Phi_C}{\Omega}\tilde{\sigma}_N(0)\right]e^{-iz_- t} \end{aligned} \tag{16}$$

Finally, the excitonic coherences in the local basis can be computed easily by performing the inverse Bloch transformation. These straightforward calculations are carried out in the next section where special attention is paid for describing qualitatively the influence of the thermal bath on the exciton dynamics.

3 Results and discussion

In this section, the previous formalism is applied for studying how a fluctuating bath modifies the way an exciton transfers a qubit state along a star graph. To

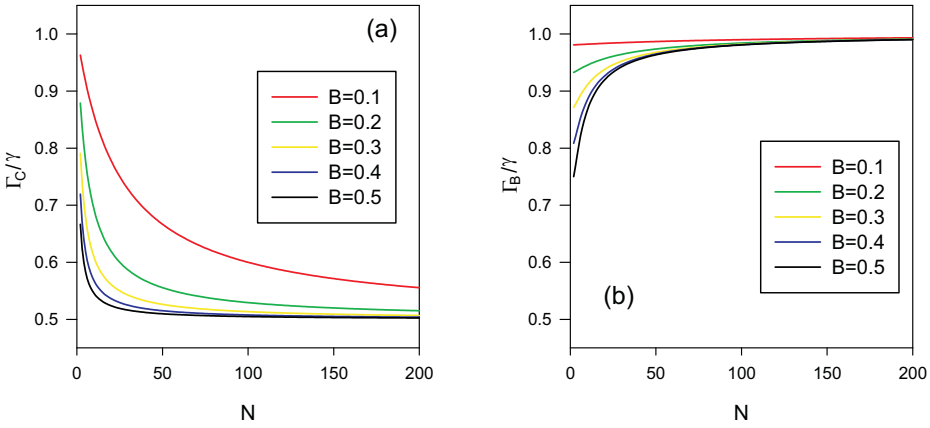

Fig. 2 Size dependence of **a** the dephasing rate Γ_C of the core state $\ell = 0$ and **b** the dephasing rate Γ_B of each branch state $\ell \neq 0$. Different B values have been considered.

proceed, the Bohr frequency ω_0 will define the energy reference ($\omega_0 = 0$) and the hopping constant Φ will stand for the energy unit. We thus focus our attention to the non-adiabatic limit (Markov limit) in which the bath correlation time is shorter than the typical time evolution of the exciton ($B < 1$). However, before analyzing on dynamical effects, we shall first characterize the relevant elements of the relaxation operator, the knowledge of which is required to solve the GME.

Figure 2 shows the size dependence of both the dephasing rate Γ_C of the core state $\ell = 0$ and the dephasing rate Γ_B of each branch state $\ell \neq 0$ (see equation (11)). Different B values have been considered. When $B = 0$, the exciton-bath coupling correlation function becomes a delta function $C(t) = 2\gamma\delta(t)$ (see equation (10)). In that case, the Markov limit is rigorously reached and $\Gamma_C = \Gamma_B = \gamma$ whatever the size of the star (not drawn). As shown in Figure 2, this is no longer the case when $B > 0$. Although the exciton interacts similarly with the bath regardless of whether it occupies a core site or a branch site, the dephasing rates become inhomogeneously distributed over the graph. Whatever the size of the star, $\Gamma_C < \Gamma_B$ indicating that the dephasing processes affecting the branch sites are faster than those that arise on the core site. Moreover, the difference between the two dephasing rates increases with the branch number. Indeed, of about $\gamma(1-2B^2)$ for $N = 1$, Γ_B increases with the star size. It converges to γ in the thermodynamic limit $N \to \infty$. By contrast, Γ_C, that is also of about $\gamma(1 - 2B^2)$ for $N = 1$, decreases with N. In the thermodynamic limit, it converges to half the asymptotic value of Γ_B and reaches $\gamma/2$.

The size dependence of the relaxation operator element Γ_I is illustrated in Figure 3 for different B values (see equation (11)). The figure reveals that $\Gamma_I \leq 0$ whatever the model parameters. It vanishes when the Markov limit is rigorously reached ($B = 0$). Otherwise, provided that $N > 2$, Γ_I increases with the size of the star. It converges to zero in the thermodynamic limit. Note that when $B \ll 1$, the amplitude of this off-diagonal element is typically two orders of magnitude smaller than the dephasing rates Γ_B and Γ_C.

Figure 4 displays the behavior of the hopping constant corrections Δ_C and Δ_B with respect to N for different B values (see equation (11)). When $B = 0$,

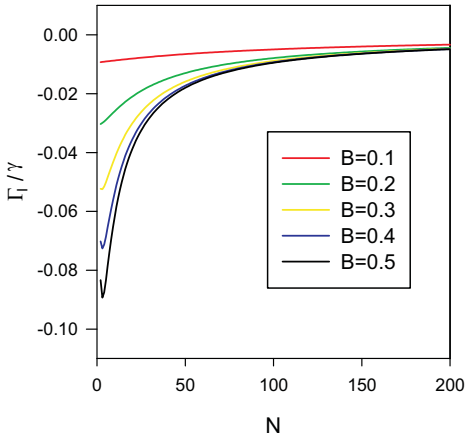

Fig. 3 Size dependence of the relaxation operator element Γ_I for different B values.

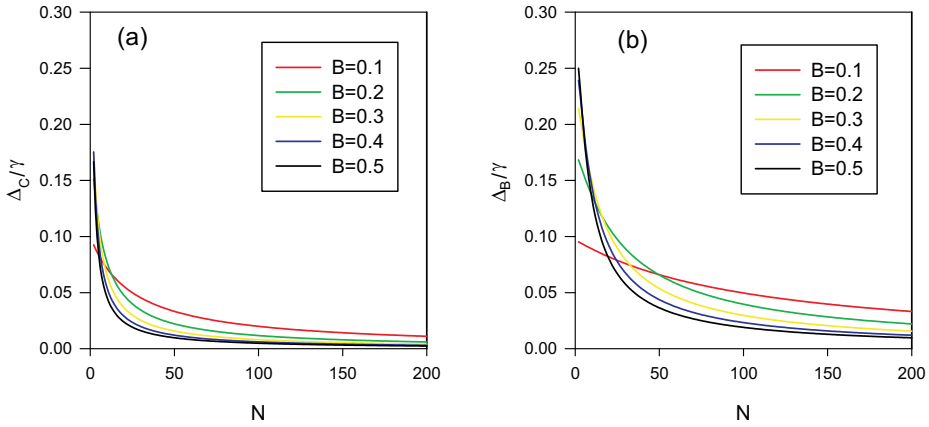

Fig. 4 Size dependence of the hopping constant corrections **a** Δ_C and **b** Δ_B for different B values.

$\Delta_C = \Delta_B = 0$ whatever the size of the star (not drawn). No dynamical frequency shift is induced by the bath when the Markov limit is rigorously reached, a behavior that results from the choice of the exciton-bath coupling correlation function whose imaginary part vanishes. As shown in Figure 4, this is no longer the case when $B > 0$. In that case, the hopping constant corrections decrease with the size of the star and they converge to zero in the thermodynamic limit. Whatever N, $\Delta_C < \Delta_B$ indicating that the probability amplitude for the exciton to tunnel from the core to the branches differs from the probability amplitude for the revert pathway. This asymmetric nature of the hopping constant corrections breaks the unitary of the excitonic propagation. Note that $\Delta_B/\Delta_C \approx 4$ when $N \to \infty$ whatever the adiabaticity.

The inhomogeneous nature of the dephasing rates and the asymmetry of the hopping constant corrections originate in the behavior of the free exciton propagator. This propagator strongly varies depending on whether the exciton occupies the core or the periphery of the star. Therefore, according to equation (9), the

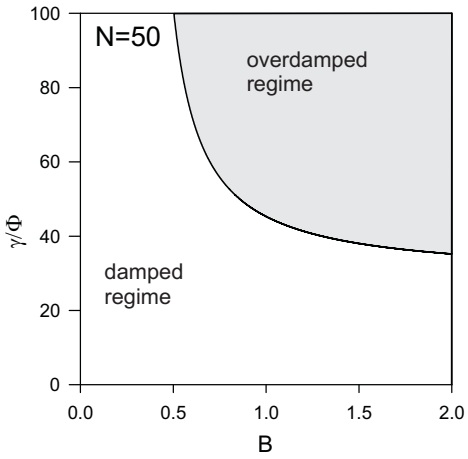

Fig. 5 Critical curve in the parameter space that discriminates between the damped regime (white part) and the overdamped regime (gray part) for $N = 50$.

different behaviors of the propagator produce different relaxation operator elements. For instance, when the exciton is initially located on the central core, a coherent delocalization arises between the core and the periphery of the star. Consequently, the propagator oscillates with frequency $\sqrt{N}\Phi$ according to the relation $|G_{00}(t)| = |\cos(\sqrt{N}\Phi t)|$ (see equation (4)). By inserting this expression into equation (9), it turns out that the dephasing rate Γ_C originates in the competition between the correlation time τ_c and the exciton Bohr frequency $\sqrt{N}\Phi$ resulting in the expression obtained in equation (11). By contrast, when the exciton is initially located on a branch site, the propagator accounts for the localization effect that arises due to the degeneracy of the spectrum. Consequently, provided that N is sufficiently large, the propagator remains quite close to unity according to the relation $|G_{00}(t)| = |1 - (1 - \cos(\sqrt{N}\Phi t))/N|$ (see equation (4)). By inserting this expression into equation (9), the dephasing rate Γ_B reduces to the integral of the coupling correlation function and it is typically of about γ, as observed in Fig. 2. Note that, the influence of the exciton propagator on the relaxation operator occurs provided that the correlation time of the thermal bath remains finite. In that case, the coupling correlation function is sufficiently long so that the relaxation operator becomes sensitive to the propagator. As a result, the dephasing rates and the hopping constant corrections also depends on the adiabaticity, a general feature previously observed in regular lattices [40]. In a marked contrast, when the Markov limit is rigorously reached ($B = \tau_c = 0$), the dephasing rates are equal to γ and the hopping constant corrections vanish.

From the knowledge of the relaxation operator elements, one can now study the effective eigenenergies z_0 and $z_\pm$ that govern the dynamics of the excitonic coherences (see equation (15)). The effective energy z_0 controls the coherence of the Bloch states $k = 1, ..., N-1$ that shows damped oscillations with frequency ω_0 and decay rate γ_0. By contrast, the effective energies $z_\pm$ describe the coherence exchanges between the core and the periphery of the star. In that case, two situations arise depending on whether Ω is real or imaginary. For real Ω values, a damped regime takes place so that the coherence exchanges show damped os-

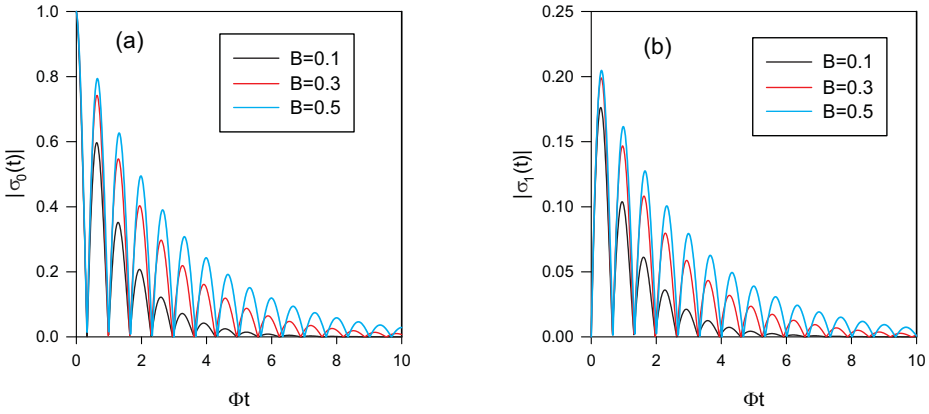

Fig. 6 Time evolution of the coherence **a** of the excited core site $\ell = 0$ and **b** of the branch site $\ell = 1$. Different B values were considered for $\gamma = \Phi$ and $N = 20$.

cillations with frequency Ω and mean decay rate $\bar{\Gamma}$. By contrast, for imaginary Ω values, an over-damped regime occurs so that the coherence exchanges no longer oscillate. As illustrated in Figure 5, the nature of the regime strongly depends on the model parameters, that is on the adiabaticity B and on the strength of exciton-bath coupling γ. Therefore, a critical curve discriminates between the two regimes. When the adiabaticity remains quite small, this curve typically scales as $\gamma/\Phi = \alpha|B-B_c|^{\nu}$, where the parameters α, B_c and ν depend on the size of the star. When N ranges between 2 and 200, the corresponding mean values are $\alpha \approx 48.76$, $B_c \approx 0.45$ and $\nu \approx 0.25$. The critical curve thus reveals that in the non-adiabatic limit ($B < 1$), the over-damped regime takes place only for very strong couplings. Such a result is inconsistent with the use of the second order perturbation theory introduced in the present paper. Consequently, in the following of the text, the over-damped regime will be disregarded.

We are now able to compute the coherences. As illustrated in Figure 6, we first consider the situation in which the excitonic qubit is initially encoded on the core site $\ell = 0$ ($\sigma_\ell(0) = \delta_{\ell 0}$). In that case, from equation (16), it is straightforward to show that the coherences are expressed as

$$\begin{aligned}\sigma_\ell(t) &= -i\frac{\Phi_B}{\sqrt{N}\Omega}e^{-i\omega_0 t}e^{-\bar{\Gamma}t}\sin(\Omega t) \quad \forall \ell = 1, ..., N \\ \sigma_0(t) &= e^{-i\omega_0 t}e^{-\bar{\Gamma}t}\left[\cos(\Omega t) + \frac{\bar{\gamma}}{\Omega}\sin(\Omega t)\right]\end{aligned} \tag{17}$$

When the coupling with the bath is turned off ($\gamma = 0$), a coherent information transfer takes place between the core site and the Bloch state $k = N$ uniformly distributed over the N branch sites (see equation (17)). The coherences $\sigma_0(t)$ and $\tilde{\sigma}_{k=N}(t)$ oscillate between ± 1 with frequency $\sqrt{N}\Phi$ indicating that a perfect QST occurs periodically. Consequently, the quantum information that is transmitted to each branch site is optimized, the maximum amplitude of the corresponding coherence being equal to $1/\sqrt{N}$ (not drawn).

For non-vanishing γ values, the coupling with the bath favors a dephasing mechanism so that the so-called damped regime occurs in the non-adiabatic weak-coupling limit. Initially equal to unity, the coherence of the core site shows damped

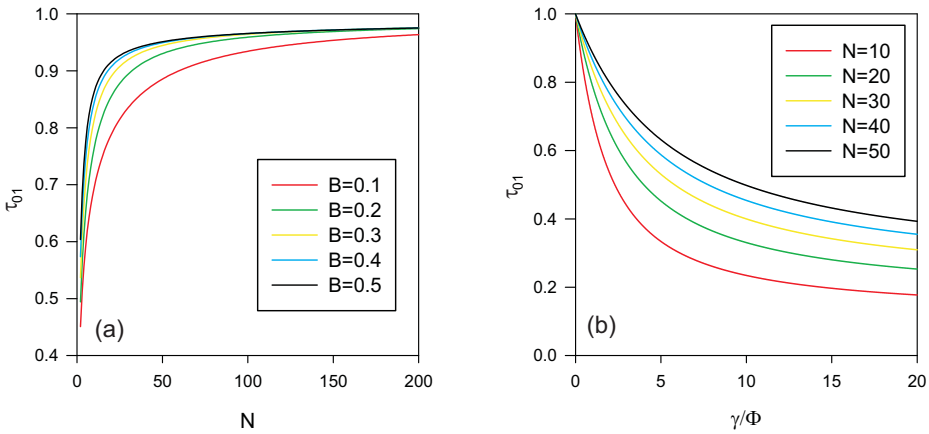

Fig. 7 **a** Size dependence of the transmission coefficient τ_{01} for different B values and for $\gamma = \Phi$. **b** Variation of the transmission coefficient τ_{01} with γ for different star size and for $B = 0.1$.

oscillations with frequency Ω and mean decay rate $\bar{\Gamma}$. It thus converges to zero in the long time limit (Fig. 6.a). However, the larger the adiabaticity is, the slower is the decoherence effect. For instance, when $B = 0.1$, the coherence of the excited site reduces to $|\sigma_0(t)| = 0.038$ at time $t = 4\Phi^{-1}$. When the adiabaticity increases to $B = 0.5$, the same coherence is almost multiplied by one order of magnitude and its reaches $|\sigma_0(t)| = 0.24$ at time $t = 4\Phi^{-1}$.

As shown in Fig. 6.b, the coherence transmitted on each branch site exhibits also damped oscillations with frequency Ω and mean decay rate $\bar{\Gamma}$. As a result, its maximum value $\sigma_{1,max}$ decreases when compared with what happens in the coherent regime. For instance, for $\gamma = 0$ and $N = 20$, $\sigma_{1,max} = 1/\sqrt{N} = 0.22$. When $\gamma = \Phi$, this maximum value reduces to $\sigma_{1,max} = 0.18$ for $B = 0.1$. Note that the adiabaticity slightly enhances the transfer and $\sigma_{1,max}$ increases as B increases. For instance, it reaches 0.20 for $B = 0.5$.

To study the influence of the model parameters on the QST, we introduce the transmission coefficient τ_{01}. It is related to the maximum value of the transmitted coherence according to the relation $\sigma_{1,max} = \tau_{01}/\sqrt{N}$. A perfect QST refers to a transmission coefficient $\tau_{01} = 1$. From equation (17), simple algebraic manipulations yield

$$\tau_{01} = \frac{\Phi_B}{\sqrt{\Phi_B \Phi_C + \gamma_B \bar{\Gamma}_C}} \exp\left[-\frac{\bar{\Gamma}}{\Omega} \arctan\left(\frac{\Omega}{\bar{\Gamma}}\right)\right] \tag{18}$$

The behavior of the transmission coefficient with respect to the model parameters is displayed in Fig. 7. Consistent with what is expected, the figure shows that τ_{01} decreases with the coupling strength indicating that the bath prevents the occurrence of any efficient QST. A detailed study of the curves displayed in Fig. 7.b reveals that τ_{01} exhibits an exponential decay with γ in the weak-coupling limit. By contrast, an algebraic decay arises for quite strong γ values. However, quite surprisingly, figure 7 clearly shows that the transmission coefficient is enhanced by both the size of the star and the adiabaticity. As illustrated in Fig. 7.a, the larger the number of branches is, the closer to unity is the transmission coefficient. For instance, for $B = 0.1$, τ_{01} is equal to 0.69, 0.93 and 0.96 for $N = 10$, 100 and 200,

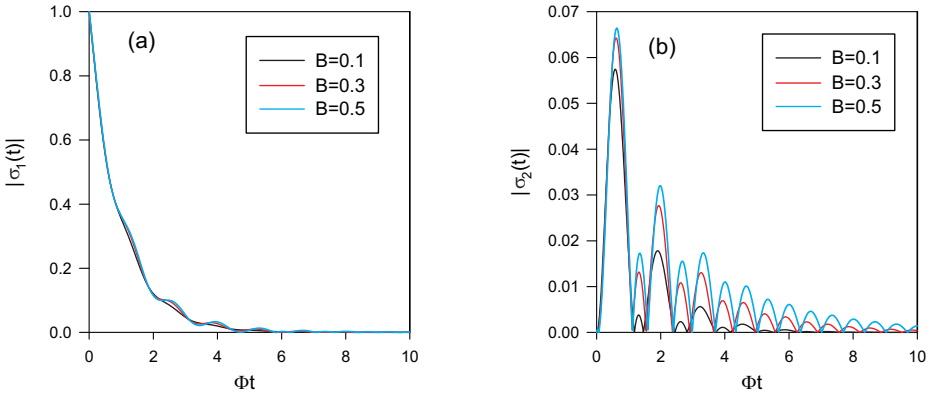

Fig. 8 Time evolution of the coherence **a** of the excited branch site $\ell = 1$ and **b** of the neighboring branch site $\ell = 2$. Different B values were considered for $\gamma = \Phi$ and $N = 20$.

respectively. This effect is more pronounced for $B = 0.5$ since the transmission coefficient reaches 0.86, 0.97 and 0.98 for $N = 10$, 100 and 200, respectively. In fact, whatever the adiabaticity, τ_{01} rapidly increases with N provided that N remains smaller than a typical value of about 40. Than, for larger sizes, τ_{01} becomes a slowly varying function that converges to unity in the thermodynamics limit.

The fact that the fidelity of the QST increases with the size of the star originates in the combination of two main effects. First, as N increases, the frequency Ω of the exchanges between the core and the periphery of the star increases as $\sqrt{N}$. In the same time, the mean rate $\bar{\Gamma}$ decreases as N increases owing to the decay of the dephasing rate Γ_C with the star size (see Fig. 3). It is expressed as

$$\bar{\Gamma} = \gamma \left[\frac{N-1}{2N} \left(\frac{1}{1+NB^2} \right) + \frac{N+1}{2N} \left(\frac{1+2NB^2}{1+4NB^2} \right) \right] \tag{19}$$

As a result, the larger N is, the shorter is the time for which the transmitted coherence becomes maximum and the smaller is the decay induced by the dephasing. Note that the increase of τ_{01} with B results from the decay of the mean dephasing rate $\bar{\Gamma}$ with the adiabaticity.

As illustrated in Figure 8, let us now focus our attention on the situation in which the excitonic qubit is initially encoded on a particular branch site $\ell = 1$ ($\sigma_\ell(0) = \delta_{\ell 1}$) . In that case, the coherences are written as

$$\begin{aligned} \sigma_\ell(t) &= e^{-i\omega_0 t} \left(\frac{N\delta_{\ell 1} - 1}{N} e^{-\gamma_0 t} + \frac{e^{-\bar{\Gamma} t}}{N} \left[\cos(\Omega t) - \frac{\bar{\gamma}}{\Omega} \sin(\Omega t) \right] \right) \quad \forall \ell \neq 0 \\ \sigma_0(t) &= -i \frac{\Phi_C}{\sqrt{N}\Omega} e^{-i\omega_0 t} e^{-\bar{\Gamma} t} \sin(\Omega t) \end{aligned} \tag{20}$$

A moment's reflection will convince the reader that the behavior of the coherence of the core site following the excitation of a branch site basically resembles the behavior of the coherence of a branch site following the excitation of the core site. Note that $\Phi_C \approx \Phi_B$ in the non-adiabatic weak-coupling limit. Because this latter situation has been studied previously, special attention will be paid now on the

characterization of the time evolution of the coherence of the excited branch site and of another branch site.

When the coupling with the bath is turned off ($\gamma = 0$), a localization phenomenon due to specific quantum interferences occurs because the star graph supports a $(N-1)$-fold degenerate eigenenergy. As a result, the coherence of the excited site $|\sigma_1(t)| = 1-(1-\cos(\Omega t))/N$ remains quite close to unity provided that the branch number is sufficiently important. As shown in Fig. 8.a, a fully different behavior arises when the coupling with the bath turns on. Dephasing takes place resulting in the decay of the excited coherence. Therefore, $|\sigma_1(t)|$ rapidly decreases with time by exhibiting small-amplitude damped oscillations. As illustrated in the figure, such a behavior is almost independent on the adiabaticity, provided that the non-adiabatic limit is reached. In fact, when B increases, the amplitude of the damped oscillations slightly increases. Moreover, we have verified that the time evolution of the excited coherence depends only slightly on the size of the star graph (not drawn).

Such a behavior results from the fact that the excited coherence involves two contributions. As shown in equation (17), the first contribution exhibits damped small-amplitude oscillations. Proportional to $1/N$, this term characterizes the coherence exchanges with the core site whose amplitude decays according to the mean rate $\bar{\Gamma}$. The second contribution is a purely exponential decaying function proportional to $(1-1/N)\exp(-\gamma_0 t)$. It accounts for the modification of the localization phenomenon due to the dephasing experienced by the degenerate Bloch states $k = 1, ..., N-1$. The corresponding coherences disappear according to the decay rate $\gamma_0 = \Gamma_B - \Gamma_I$ that is almost insensitive to B and N. In that context, provided that N is sufficiently large, this latter contribution dominates resulting in the almost purely exponential decay observed in Fig. 8.a.

Owing to the localization process, the coherence transmitted on a neighboring branch site $\ell = 2$ exhibits small-amplitude oscillations whose maximum value is $\sigma_{2,max} = 2/N$ when the coupling with the bath is turned off. As shown in Fig. 8.b, when this coupling switches on, dephasing-limited coherent motion reinforces the localization effect. The coherence shows damped oscillations whose maximum value becomes smaller than the reference value $2/N$. For instance, for $N = 20$, $\sigma_{2,max} = 2/N = 0.1$ when $\gamma = 0$ whereas $\sigma_{2,max} = 0.057$ when $\gamma = \Phi$ and $B = 0.1$. Note that, as observed previously, the adiabaticity slightly enhances the transfer and $\sigma_{2,max}$ increases as B increases. It reaches 0.064 and 0.066 for $B = 0.3$ and $B = 0.5$, respectively.

At this step, let τ_{12} define the transmission coefficient connected to the maximum value of the transmitted coherence according to the relation $\sigma_{2,max} = 2\tau_{12}/N$. Note that no analytical expression can be extracted form equation (20). The behavior of τ_{12} with respect to the model parameters is illustrated in Fig. 9. The figure reveals that τ_{12} decreases with the coupling strength γ in agreement with the fact that dephasing enhances the localization process. However, as previously observed in figure 7, τ_{12} increases with both the size of the star and the adiabaticity. In particular, the larger the number of branches is, the closer to unity is the transmission coefficient (see Fig. 9.a). For instance, for $B = 0.1$, τ_{12} is equal to 0.45, 0.80 and 0.86 for $N = 10$, 100 and 200, respectively. This effect is slightly enhanced when the adiabaticity increases and for $B = 0.5$, τ_{12} reaches 0.58, 0.83 and 0.87 for $N = 10$, 100 and 200, respectively. In fact, whatever B, the curve τ_{12} vs N shows two regimes. Provided that N remains smaller than a typical value

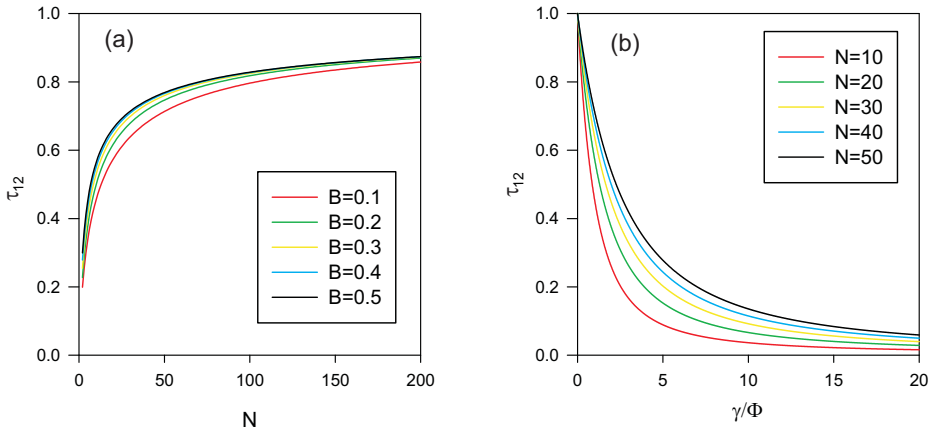

Fig. 9 **a** Size dependence of the transmission coefficient τ_{12} for different B values and for $\gamma = \Phi$. **b** Variation of the transmission coefficient τ_{12} with γ for different star size and for $B = 0.1$.

of about 40, τ_{12} rapidly increases with N. By contrast, for larger N values, τ_{21} becomes a slowly varying function of the star size that finally converges to unity in the thermodynamics limit.

Although no analytical expression of the transmission coefficient τ_{12} can be obtained, we have verified that its N dependence is quite similar to the N dependence of the coefficient τ_{01} defined in equation (18). It mainly results from the increase of the exciton Bohr frequency Ω with the branch number. Consequently, the larger N is, the shorter is the time for which the transmitted coherence becomes maximum and the smaller is the decay induced by the dephasing. As a result, the transmission coefficient is optimized as the size of the star increases.

4 Conclusion

In the present paper, a phenomenological model has been introduced for studying how a fluctuating bath modifies the way an exciton promotes QST on a star graph. To proceed, a GME was established for describing the time evolution of specific elements of the exciton RDM. These elements, called coherences, characterize the ability of the exciton to develop qubit states that are superimpositions involving the vacuum and the local one-exciton states. In the GME, the influence of the thermal bath was encoded in a relaxation operator whose key elements define the well-known dephasing rates and hopping constant corrections. Within the non-adiabatic weak-coupling limit (Markov approximation), the GME was solved exactly by taking advantage of the fact that it possesses discrete rotational symmetry. We were thus able to obtain analytical expressions for both the dephasing rates and the hopping constant corrections as well as for the excitonic coherences.

In that context, it has been shown that when the exciton-bath coupling is turned off, the coherences behave as the free exciton propagator whose properties depend on the initial position of the exciton. When the exciton is initially located on the core site, a coherent delocalization arises between the core and the periphery of the graph. By contrast, when the exciton occupies initially a branch site, a

localization phenomenon arises due to specific quantum interferences that result from the degeneracy of the spectrum of the star graph. When the exciton-bath coupling is turned on, a fully different behavior takes place. Indeed, as expected from standard theories, dephasing-limited coherent motion occurs. The thermal bath is thus responsible for quantum decoherence that strongly impoverishes the efficiency of any quantum communication protocol. Therefore, when the exciton is initially located on the core site, the dephasing favors a localization effect that prevents the occurrence of a perfect QST between the core and the periphery of the graph. Similarly, when the exciton initially occupies a branch site, the dephasing enhances the localization that originates in the degeneracy of the star spectrum.

However, when compared with what happens on regular lattices, our study has revealed that the dephasing processes and the QST fidelity are very sensitive to the topology of the graph and to the number of branches that form the star. These features originate in the nature of the relaxation operator that depends on the free exciton propagator provided that the bath correlation time remains short but finite. As a consequence, it has been shown that the dephasing rates are inhomogeneously distributed over the graph. The dephasing processes that affect the branch sites are thus faster than those that arise on the core site, such an effect being enhanced as the size of the star increases. Moreover, the bath produces an asymmetric correction of the exciton hopping constant that breaks the unitary of the excitonic propagation. Finally, the QST fidelity is optimized as the size of the star increases because the frequency of the exchanges between the core and the periphery increases with the size whereas the mean decay rate that governs these exchanges decreases. As a result, the larger the size is, the shorter is the time for which the QST becomes optimized and the smaller is the decay induced by the dephasing.

References

1. Bennet, C.H., DiVincenzo, D.P.: Quantum information and computation. Nature (London) **404**, 247 (2000)
2. Burgarth, D.:Quantum state transfer and time-dependent disorder in Quantum Chains. Eur. Phys. J. Spec. Top. **151**, 147 (2007)
3. Bose, S.: Quantum Communication through an Unmodulated Spin Chain. Phys. Rev. Lett. **91**, 207901 (2003)
4. Christandl, M., Datta, N., Ekert, A., Landahl, A.J.: Perfect State Transfer in Quantum Spin Networks. Phys. Rev. Lett. **92**, 187902 (2004)
5. Bose, S.:Quantum communication through spin chain dynamics: an introductory overview. Contemp. Phys. **48**, 13 (2007)
6. Semio, F.L., Furuya, K., Milburn, G.J.: Vibration-enhanced quantum transport. New J. Phys. **12**, 083033 (2010)
7. Reslen, J., Bose, S.: End-to-end entanglement in Bose-Hubbard chains. Phys. Rev. A **80**, 012330 (2009)
8. Haffner, H., Roos, C.F., Blatt, R.: Quantum computing with trapped ions. Phys. Rep. **469**, 155 (2008)
9. Huo, M.X., Li, Y., Song, Z., Sun, C.P.: The Peierls distorted chain as a quantum data bus for quantum state transfer . Eur. Phys. Lett. **84**, 30004 (2008)
10. M. Plenio, B., Hartley, J., Eisert, J.: Dynamics and manipulation of entanglement in coupled harmonic systems with many degrees of freedom. New J. Phys. **6**, 36 (2004)
11. Pouthier, V.: Vibrational exciton mediated quantum state transfer: Simple model. Phys. Rev. B **85**, 214303 (2012)
12. Pouthier, V.: Vibrons in finite size molecular lattices: a route for high-fidelity quantum state transfer at room temperature. J. Phys.: Condens. Matter **24**, 445401 (2012)

13. Pouthier, V.: A qubit coupled with confined phonons: The interplay between true and fake decoherence. J. Chem. Phys. **139**, 054103 (2013)
14. Mulken, O., Bierbaum, V., Blumen, A.: Coherent exciton transport in dendrimers and continuous-time quantum walks. J. Chem. Phys. **124**, 124905 (2006)
15. Agliari, E., Blumen, A., Mulken, O.: Quantum-walk approach to searching on fractal structures. Phys. Rev. A **82**, 012305 (2010)
16. Mulken, O., Blumen, A.: Continuous-time quantum walks: Models for coherent transport on complex networks. Phys. Rep. **502**, 37 (2011)
17. Pouthier, V.: Exciton localization-delocalization transition in an extended dendrimer. J. Chem. Phys. **139**, 234111 (2013)
18. Pouthier, V.: Disorder-enhanced exciton delocalization in an extended dendrimer. Phys. Rev. E **90**, 022818 (2014)
19. Astruc, D., Boisselier, E., Ornelas, C.: Dendrimers designed for functions: from physical, photophysical, and supramolecular properties to applications in sensing, catalysis, molecular electronics, photonics, and nanomedicine. Chem. Rev. **110**, 1857 (2010)
20. Mukamel, S.: Trees to trap photons. Nature **388**, 425 (1997)
21. Childs, A.M.: Universal Computation by Quantum Walk. Phys. Rev. Lett. **102**, 180501 (2009)
22. Childs, A.M., Goldstone, J.: Spatial search by quantum walk. Phys. Rev. A **70**, 022314 (2004)
23. Farhi, E., Goldstone, J., Gutmann, S.: A Quantum Algorithm for the Hamiltonian NAND Tree. Theory Comput. **4**, 169 (2008)
24. Childs, A.M., Farhi, E. and Gutmann, S.: An Example of the Difference Between Quantum and Classical Random Walks. Quantum Inf. Process **1**, 35 (2002)
25. Rebentrost, P., Mohseni, M., Kassal, I., Lloyd, S., Aspuru-Guzik A.: Environment-assisted quantum transport. New. J. Phys. **11**, 033003 (2009)
26. Steven R. Jackson, Teng Jian Khoo, and Frederick W. Strauch: Quantum walks on trees with disorder: Decay, diffusion, and localization. Phys. Rev. A **86**, 022335 (2012)
27. Cardoso, A.L., Andrade, R.F.S., Souza, A.M.C.: Localization properties of a tight-binding electronic model on the Apollonian network. Phys. Rev. B **78**, 214202 (2008)
28. Xu, X.P., Li, W., Liu, F.: Coherent transport on Apollonian networks and continuous-time quantum walks. Phys. Rev. E **78**, 052103 (2008)
29. Salimi, S.: Continuous-time quantum walks on star graphs. Ann. Phys.**324**, 1185 (2009)
30. Xu, X.P.: Exact analytical results for quantum walks on star graphs. J. Phys. A: Math. Theor. **42**, 115205 (2009)
31. Ziletti, A., Borgonovi, F., Celardo, G.L., Izrailev, F.M., Kaplan, L., Zelevinsky, V. G.: Coherent transport in multibranch quantum circuits. Phys. Rev. B **85**, 052201 (2012)
32. Anishchenko, A., Blumen, A., Mulken, O.: Enhancing the spreading of quantum walks on star graphs by additional bonds. Quantum Inf. Process **11**, 1273 (2012)
33. May, V., Kuhn, O.: Charge and Energy Transfer Dynamics in Molecular Systems. Wiley-VCH Verlag, Berlin (2000)
34. Breuer, H.P., Petruccione, F.: The theory of open quantum systems. Oxford University Press, New York (2007)
35. Pouthier, V.: Phonon anharmonicity-induced decoherence slowing down in excitonphonon systems. J. Phys.: Condens. Matter **22**, 25560(2010)
36. Haken H., Strobl G.: An exactly solvable model for coherent and incoherent exciton motion. Z. Phys. **262**, 135 (1973)
37. Blumen, A., Silbey, R.: Exciton line shapes and migration with stochastic exciton lattice coupling. J. Chem. Phys. **69**, 3589 (1978)
38. Jackson, B., Silbey, R.: Line shapes and transport for excitons with stochastic coupling. J. Chem. Phys. **75**, 3293 (1981)
39. Rips I.: Stochastic models of exciton transport: The Haken-Strobl model. Phys. Rev. E **47**, 67 (1993)
40. Pfluegl, W., Palenberg, M.A., Silbey, R.: Diffusion coefficient for disordered systems with coupled coherent and incoherent transport in one dimension. J. Chem. Phys. **113**, 5632 (2000)
41. Xu, X.P.: Coherent exciton transport and trapping on long-range interacting cycles. Phys. Rev. E **79**, 011117 (2009)
42. Mendonca, P.E.M.F., Napolitano, R.J., Marchiolli, M.A., Foster, C.J., Liang, Y.C.: Alternative fidelity measure between quantum states. Phys. Rev. A **78**, 052330 (2008)